DYNAMICS OF SUCCESSIVE DROP IMPACTS ON A SOLID SURFACE

MICHAEL MEADEN & EMILY MEISSEN

Abstract. This paper compares the impact and spread velocities of a liquid drop impacting on a solid surface. It also studies a second, consecutive drop by looking at the maximum spread factors reached by the first and second drops and the number of secondary droplets (a characterization of splashing) caused by the impact of the second drop.

1. Introduction

Scientists have studied a liquid drop impacting a solid or liquid surface for over one hundred years. Worthington [5] pioneered the subject in the early 20th century by investigating drop impacts in a deep fluid using high speed photography. Research in macro liquid drop impacts on solid surfaces and liquid films is helpful in understanding the growth and splashing patterns of raindrops, which has important implications for soil erosion as well as ice accumulation on power lines and aircraft. Research has focused on a single drop impacting a solid surface or a uniform liquid film (see Yarin [6] for a comprehensive review); there is little regarding multiple drops impacting successively on a solid surface. In this paper, proposed scaling laws are experimentally tested and extensions to a second, consecutive impact are explored.

The *lamella* is defined as the primary part of the liquid film created after impact. When a single drop impacts a surface, the phenomena of *fingering* – a quasi-periodic unevenness of the boundary of the lamella – and *splashing* – a breaking-off of such "fingers" from the lamella into the air or along the surface (see Figure 1) – can occur. The fingers which break off during splashing are referred to as *secondary droplets*. Such phenomena occur when multiple drops impact successively on a surface as well, though this case is largely unexplored.

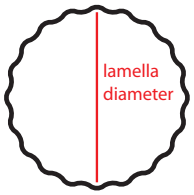

(A) Fingering, or unevenness of the boundary.

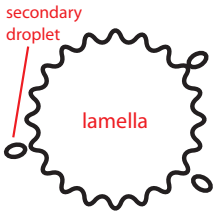

(B) Splashing, or breaking off of fingers from the lamella.

Figure 1. Phenomena occurring from impacting liquid drops.

d	Drop Diameter	v	Characteristic Velocity
σ	Surface Tension	μ	Dynamic Viscosity
ρ	Fluid Density	g	Gravitational Acceleration

Table 1. Relevant parameters.

Weber Number	$We = \frac{\rho d v^2}{\sigma}$	Inertia vs. Surface Tension
Reynolds Number	$Re = \frac{\rho d v}{\mu}$	Inertia vs. Viscous Forces
Bond Number	$Bo = \frac{\rho g d^2}{\sigma}$	Gravitation vs. Surface Tension
Froude Number	$Fr = \frac{v^2}{gd}$	Inertia vs. Gravitation

Table 2. Non-dimensional groups using parameters from Table 1.

The common non-dimensional groups for this topic, using the relevant parameters listed in Table 1, are listed in Table 2. When the Bond number is less than one, as was the case in

Date: December 15, 2011.

the experiments presented, gravitational forces are negligible, and the Weber and Reynolds numbers are considered to be the most important non-dimensional groups [4].

Many liquid drop impact phenomena are related to the Reynolds and Weber numbers, which can be calculated using either the impact velocity or the spread velocity. Most previous studies have used the former. Finding the correlation between these two velocities would explain how the relations found depend on which velocity is used. An investigation of the relationship between the *impact velocity* of a drop and the *spread velocity* of the lamella directly after impact is presented. The *maximum spread factor*, ξ, defined as the ratio of the maximum lamella diameter to the drop diameter before impact, is also found for both the first and second drop impacts. Many scaling relationships, both theoretical and empirical, have been proposed for this maximum spread factor, and a vast majority of these relate the spread factor to Re and We, though many of these relate specifically to certain types of fluids or experimental conditions. The splashing behavior is characterized by the number of secondary droplets, N, caused by the second impact, and possible scaling relationships for N is also explored.

For all experiments presented, the impact velocity was varied by adjusting the height from which the water droplets were released. For water, this gave a range of approximately 100 to 300 for the impact Weber number; and a range of approximately 5,500 to 10,000 for the impact Reynolds number. For ethanol, this gave a range of approximately 150 to 600 for the impact Weber number; and a range of approximately 2,500 and 5,000 for the impact Reynolds number.

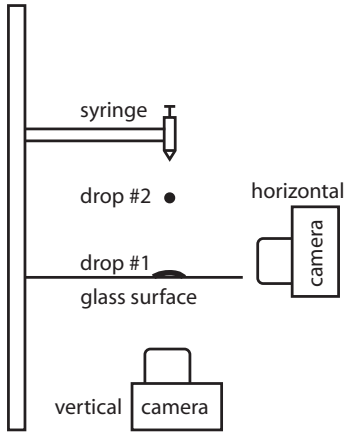

FIGURE 2.
Experimental setup. Most experiments used a vertical camera view. Measuring the impact velocity required a horizontal camera view.

2. Experimental Methodology

An elevated syringe with a 16 gauge needle (corresponding to an outer diameter of 1.62 mm) was used to release successive water drops to orthogonally impact a glass surface (see Figure 2). The height from which the drop was released was measured from the glass surface to the tip of the syringe. A high-speed camera was used to capture videos at 2000 fps. The glass surface was cleaned with distilled water and dried with a micro-fiber cloth between trials. The data for each height were averaged over four trials.

The relevant parameters for analysis are listed in Table 1. The surface tension, dynamic viscosity, and density of water at room temperature are known to be 0.07197 N/m, 0.00089 Ns/m^2, and 1000 kg/m^3, respectively. The respective values for ethanol at room temperature are known to be 0.02227 N/m, 0.001074 Ns/m^2, and 789 kg/m^3.

2.1. *Drop Diameter.* To determine the average water drop diameter, twenty drops were sampled out and the mass of the total pool was measured after each drop. The volume of each drop, V, was deterimed based on the difference in mass and the known fluid density. Assuming a spherical drop, the drop diameter was calculated using $d = \sqrt[3]{6V/\pi}$. Averaging over the 20 drops, the average water drop diameter was 0.3778 cm with a standard deviation of 0.0070 cm – less than two percent of the average diameter. Similarly, the average drop diameter for ethanol was found to be 0.2761 cm with a standard deviation of 0.0026 cm. These values were used when calculating the Weber number and maximum spread factor.

2.2. *Maximum Spread Factor.* Recall the definition of the maximum spread factor to be the ratio of the *average diameter of the lamella at the time when this is maximized* to the *drop diameter* (found above). To find this, a sequence of images was taken with the vertical camera view. Taking the frame in which the size of the lamella stopped increasing, an edge-detection algorithm (see Appendix) calculated the area, A, of the

(A) original (B) edge() (C) dilate (D) fill/erode

FIGURE 3. Images produced using the edge-detection algorithm to find the maximum spread factor. Height of 150mm, drop 1. Maximum lamella diameter: 0.012 m.

lamella. The diameter was then calculated as $d_{max} = 2\sqrt{A/\pi}$. This process was repeated for the second drop.

The edge-detection algorithm first used `MATLAB`'s `edge()` routine. In most cases, this did not detect the full boundary of the drop. The algorithm then dilated this region to merge the boundary and create a connected component (the lamella). The largest connected component was taken and filled. Then the boundary was eroded to undo the growth of the boundary caused by the dilation (see Figure 3). Summing the pixels in the region gave the total area encapsulated. This method worked in all cases for the first drop in which the lamella had a visible boundary. The second drop usually had regions of the boundary which were barely visible to the human eye. After manually drawing in these parts of the boundary, the algorithm successfully determined the diameter.

2.3. *Impact Velocity.* To determine the impact velocity, a sequence of images was taken from the horizontal camera view. This view showed the final 5 cm of the fall before the water drop impacted the glass surface. `Tracker` [1], an open-source program, was then used to gather data from the sequence. The program's auto-track feature tracked the position of a selected high-contrast region on the drop. The position data collected was used to calculate the impact velocity. Figure 4 shows data for a typical trial.

2.4. *Spread Velocity.* `Tracker` was used to determine the initial spread velocity of the lamella from the vertical camera view. Defining the origin to be at the center of the drop impact, the edge of the lamella along an axis was tracked manually in each frame until the lamella stopped spreading. Figure 5 shows sample position data for a given trial.

2.5. *Splashing Behavior.* Using the image sequences from the vertical camera view, the number of secondary droplets which completely disconnected from the lamella during the second drop's impact was counted. This number characterized the splashing behavior for a given Weber number. Secondary droplets could have arisen from droplets being jettisoned from the lamella immediately upon impact of the second drop or from fingers disconnecting from the lamella during spreading. Liquid residue left on the glass after the lamella receded was not considered a secondary droplet.

3. Experimental Results

3.1. *Relating Impact Velocity and Spreading Velocity.* Tracking the impacting drop from the horizontal camera view revealed a nearly linear position curve over time, shown in Figure 4. The impact velocity was taken as the average velocity over the final ten tracked frames. The vertical perspective videos used to measure the initial spread velocity of the lamella showed only 9-12 frames between when the drop first impacted the surface and when the lamella stopped spreading. Because the lamella decelerates rapidly, the initial spread velocity was calculated using only the first two frames of impact.

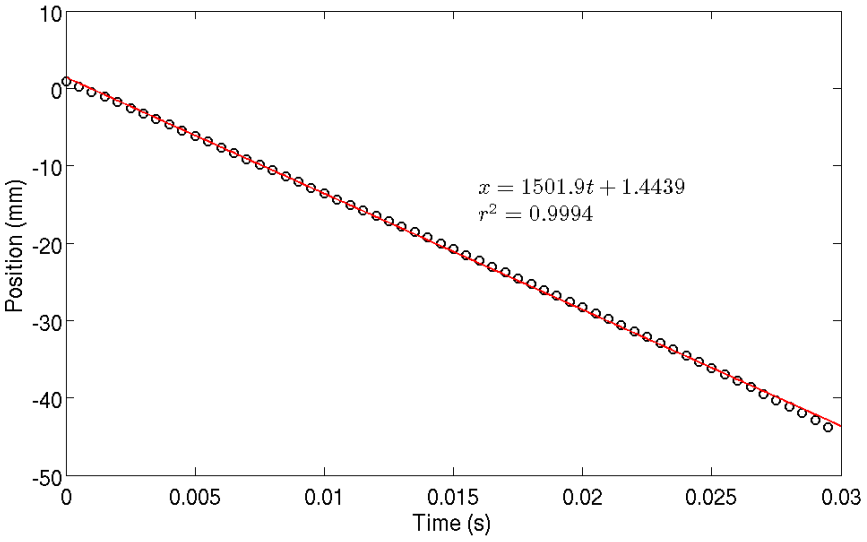

FIGURE 4. Example of position data given by `Tracker` for drop height of 135 mm, trial 1 when tracking a falling water droplet. The coordinate axis was specified such that the origin was approximately in the center of the drop and it moved along the negative x-axis. The calculation of the impact velocity used the final ten points.

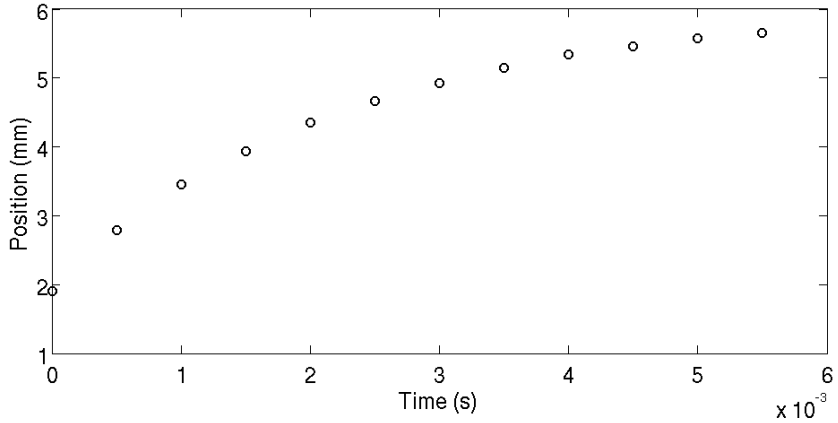

FIGURE 5. Example of tracking data given by `Tracker` for drop height of 135 mm, trial 1 when tracking the rim of the lamella for a water droplet impact. The calculation of the spread velocity used the first two points.

The measured impact velocities are shown in Figure 6 and the measured spread velocities are shown in Figure 7. The position of measured impact velocities relative to the predicted values assuming no air resistance (shown as the theoretical fit in Figure 6) implies that there was both air resistance and a non-zero initial velocity, giving the ethanol data a higher predicted velocity due to a smaller drop size. The curves shown in Figures 6 and 7 relate the impact and spread velocities to the square root of the height from which the drop is released, which we infer from the theoretical fit in Figure 6. If these relations are true, we would expect that the ratio of the spread velocity to the impact velocity, shown in Figure 8, would be linear.

3.2. *Maximum Spread Factor.* Using the edge-detection method to find the maximum diameter of the lamella, a strong positive correlation was found between Weber number and the maximum spread factor

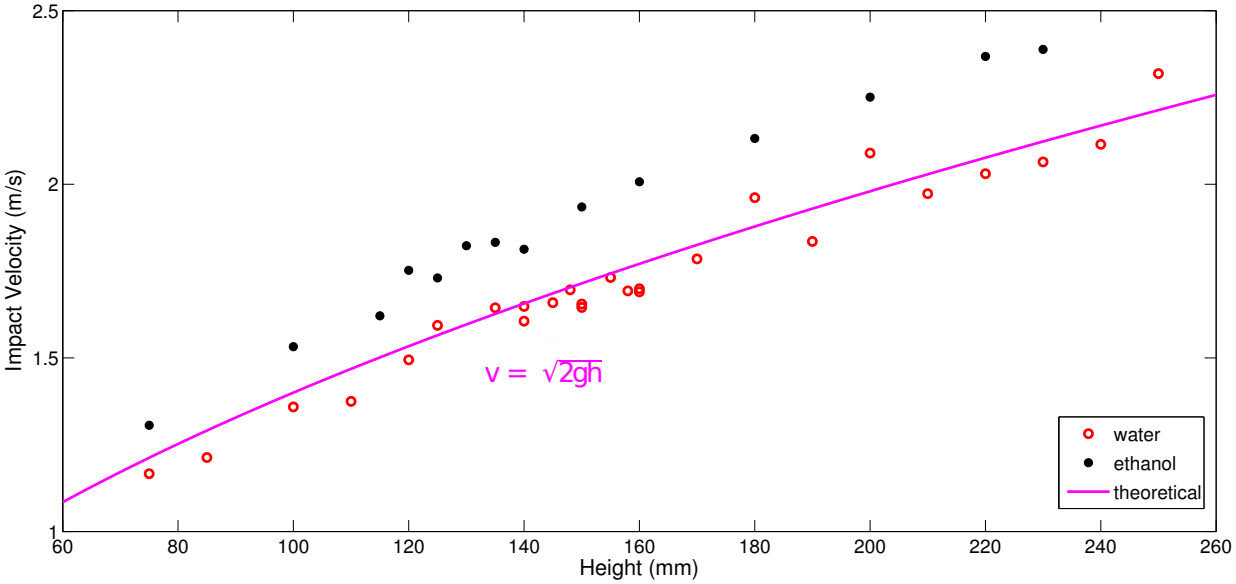

FIGURE 6. Impact Velocity vs. Height. The theoretical curve corresponds to the predicted impact velocity assuming no air resistance and zero initial velocity.

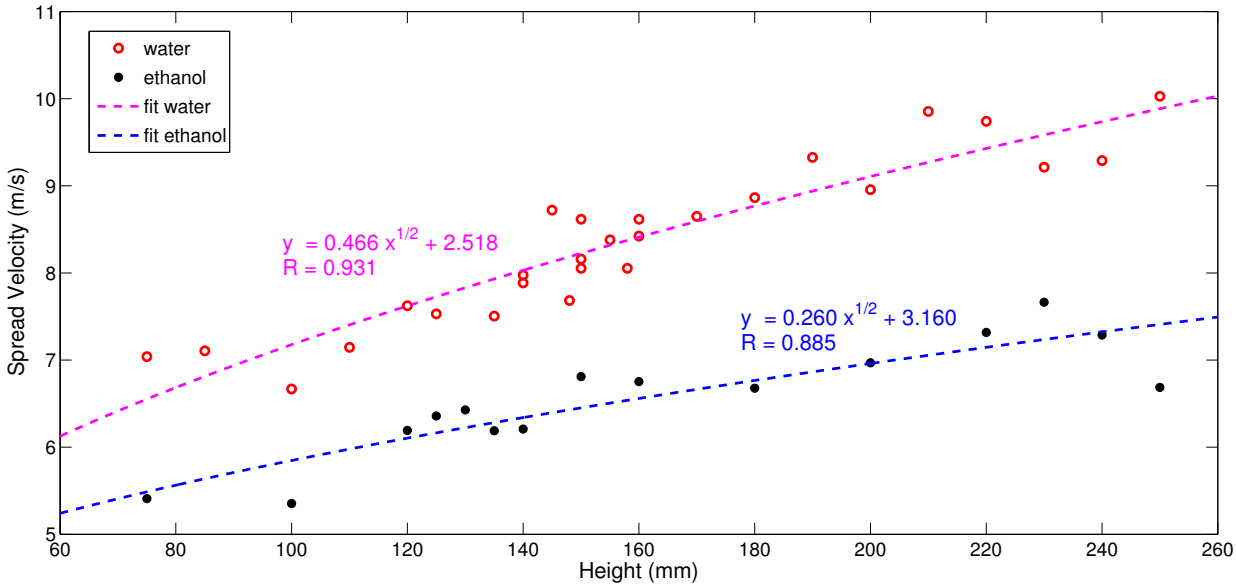

FIGURE 7. Spread Velocity vs. Height. The fits relate the spread velocity to the square root of the height, a relation inferred from the predicted fit in Figure 6

.

for the first and second drops, as shown in Figure 9. The difference between the spread factors of the first and second drop appeared to be approximately constant for the regime considered. The ethanol and water data appear to have distinct trends when viewed against We.

3.3. *Splashing Behavior.* There was a positive correlation between the number of secondary droplets and both the Weber number and the Reynolds number. Experimental conditions, such as temperature and

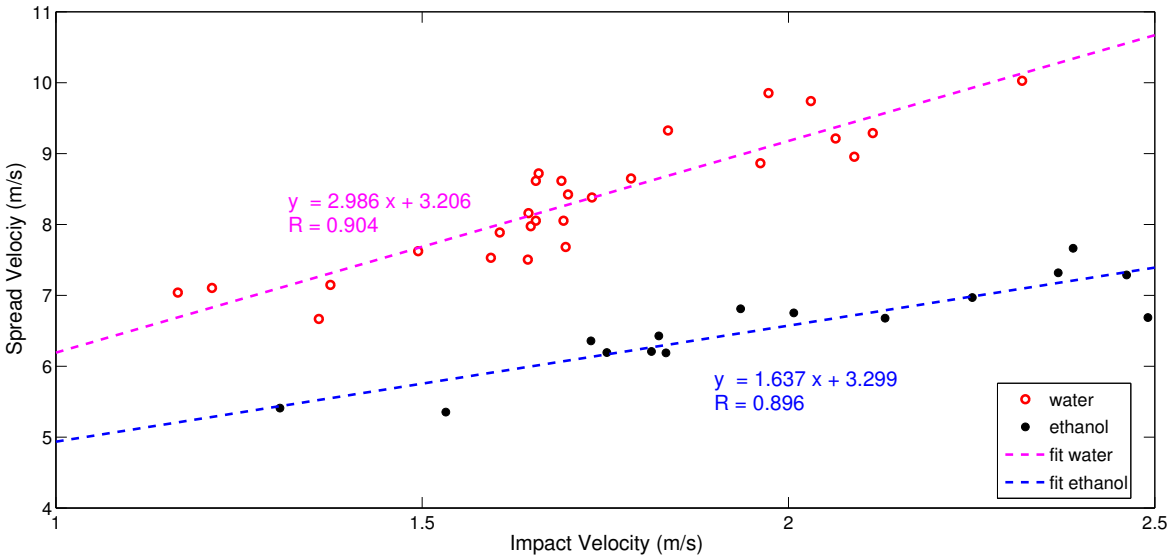

FIGURE 8. Spread Velocity vs. Impact Velocity. We expect a linear relationship, as mentioned in Results and Discussion.

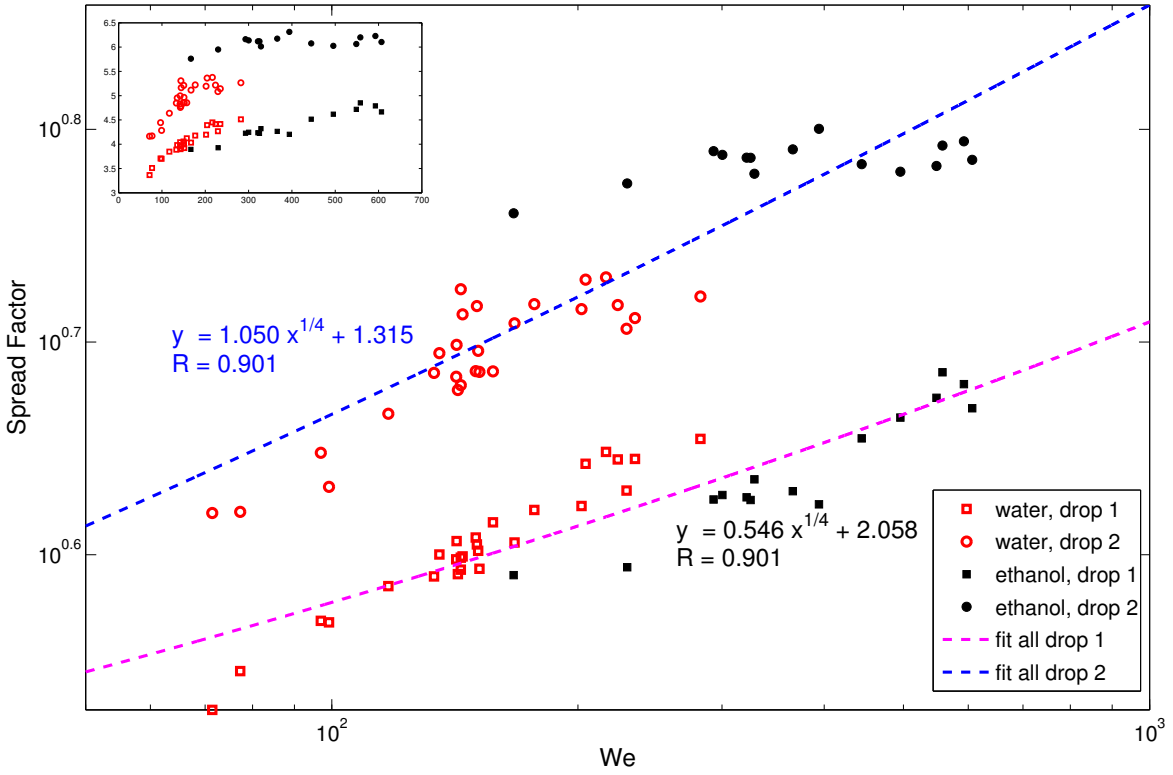

FIGURE 9. Maximum spread factor vs. Weber number loglog plot. The smaller plot shows a non-loglog plot. Both drop 1 and drop 2 exhibit a positive correlation with the Weber number for ethanol and water data. The water and ethanol data do not coincide well, implying some other factor may also be used to determine the spread factor.

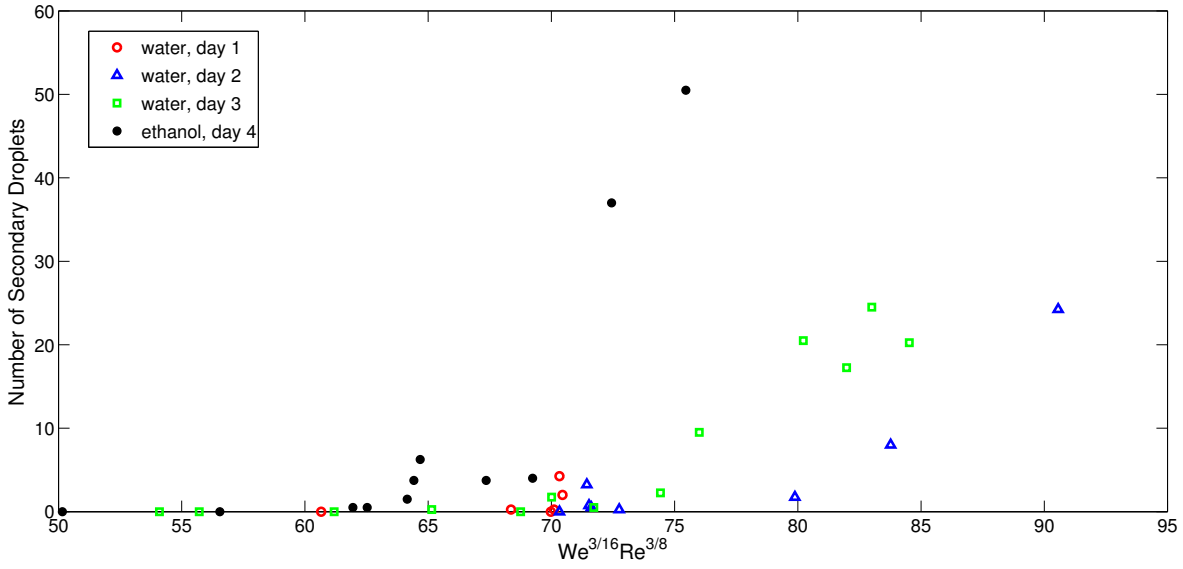

FIGURE 10. Number of secondary droplets vs. $We^{3/16}Re^{3/8}$. Note that the splashing thresholds and data do not align well between the ethanol and water data, implying that there is some other factor which may be used to predict the number of secondary droplets.

humidity which changed between testing days, appears to have shifted the splashing threshold, which made it difficult to resolve a precise trend. Marmanis and Thoroddsen [3] predict the number of fingers to scale with $We^{3/16}Re^{3/8}$. Because secondary droplets result from fingers detaching from the lamella, the number of secondary droplets should also follow this relationship. Figure 10 shows a plot of the number of secondary droplets against $We^{3/16}Re^{3/8}$. This relationship does not give an accurate representation of the number of secondary droplets since the ethanol data shows a greater number of secondary droplets for smaller values of $\mathrm{We}^{3/16}\mathrm{Re}^{3/8}$. Figure 11, however, shows that the number of secondary droplets may instead scale with $(WeRe)^{3/16}$; when plotted against this, the ethanol and water data better coincide and have similar splashing thresholds.

4. Discussion

Throughout data acquisition and analysis, many inconsistencies in the data became apparent. These inconsistencies were most likely the result of variations in experimental conditions, as well as possible human error, or possible error in the tracking and edge-detection methods. Experimental variations may have occurred in: drop size, height measurement, angle of impact, initial velocity, room temperature and humidity (which affects ρ and σ), location of second drop impact relative to first, time between impacts, and the shape of the drop during fall or at impact. While most of these variations were likely very small, they may have still had an effect on the data, especially near critical cases, such as the splashing threshold. General trends in the data, however, could still be observed. The following section offers some discussion and theoretical background related to the results seen above.

4.1. *Impact vs. Spread Velocity.* Roisman [4] provides a theoretical model of the initial phase of impact of a liquid drop on a solid surface. Figure 12 shows a schematic of the drop during the initial phase of impact, assumed to be valid from $t = 0$, when the droplet first touches the surface, until the *crash time* $t_c = d/U_0$, where d is the initial drop diameter and U_0 is the impact velocity. Figure 12 shows three distinct regions of the liquid during this time. Region 1 is assumed to be unperturbed and behaves as a rigid body moving down towards the surface with velocity U_0. This causes a high pressure gradient to form in region 2, which

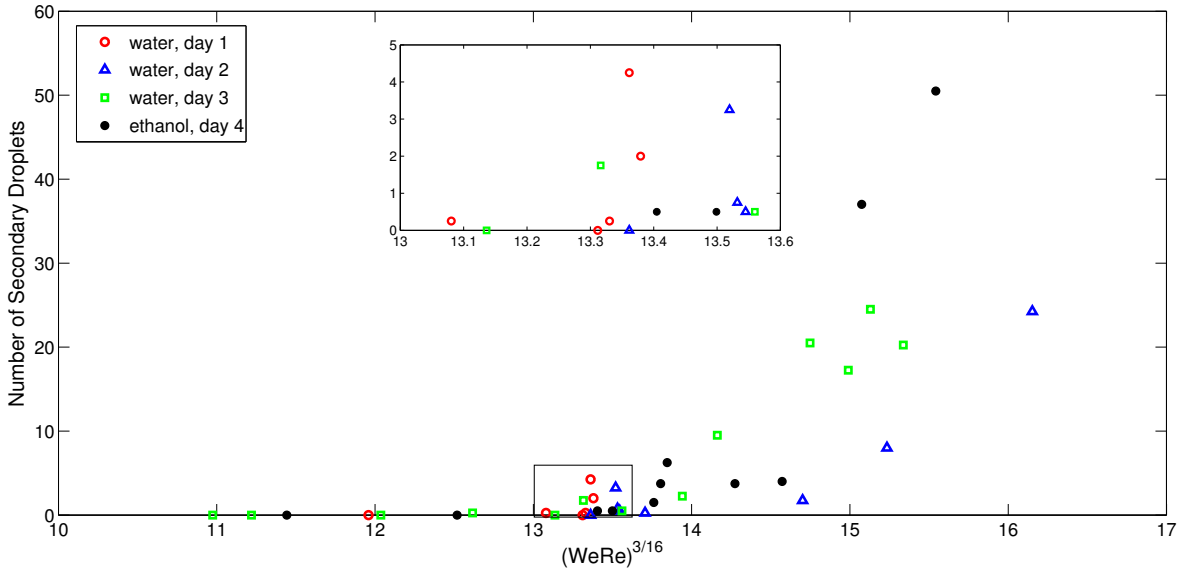

FIGURE 11. Number of secondary droplets vs. $(WeRe)^{3/16}$. Here, the splashing thresholds of the water and ethanol data align well (given sources of error between trials). The smaller plot zooms in on the data near the splashing threshold.

forces liquid radially outward into the lamella in region 3, where pressure is assumed to be uniform over the entire region.

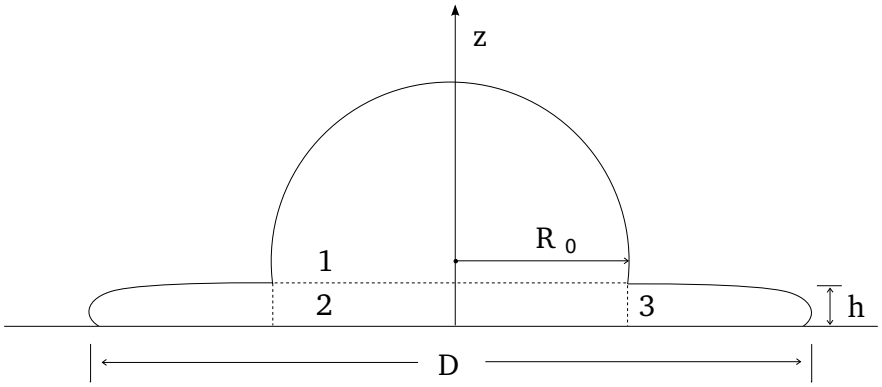

FIGURE 12. Schematic of drop impact during the initial phase of impact.

The equations of motion for region 2 dictate the relationship between the impact velocity and the spread velocity. If inertial terms are neglected, this region can be modeled as a viscous creeping flow between two approaching discs. Using cylindrical polar coordinates, the Navier-Stokes equations and the continuity equation for fluid flow give the equations of motion

$$\mu\frac{\partial^2 v_r}{\partial z^2} = \frac{\partial p}{\partial r} \qquad \frac{\partial p}{\partial z} = 0 \qquad \frac{1}{r}\frac{\partial (r v_r)}{\partial r} + \frac{\partial v_z}{\partial z} = 0$$

with boundary conditions

$$v_r = v_z = 0 \text{ for } z = 0 \qquad v_r = 0,\ v_z = -U_0 \text{ for } z = h \qquad p = p_0 \text{ for } r = R$$

where p is pressure and R is the radius of region 2. Solving this system yields an expression for the radial velocity in terms of the impact velocity:

$$v_r = \frac{3U_0}{h^3} rz(h - z).$$

For a given height z and radius r, the relationship between the radial velocity and the impact velocity is predicted to be linear by Roisman's model; for sufficiently small time, the radial velocity at the edge of the lamella corresponds to the initial spread velocity, implying a linear relationship between the impact and initial spread velocities. The observed relationship between the initial spread velocity and the impact velocity shown in Figure 8 appears to support this theoretical prediction of a linear relationship reasonably well, though the experimental results show that the slope of the linear fit is not a constant for all liquids, indicating a possible dependence on fluid properties. It is important to note that Roisman's model is valid only when working with sufficiently large impact velocities that are still less than the splashing threshold for a single drop and only when the ratio of inertial forces to viscous forces is small. While these conditions are met for the liquids and velocities considered in this paper, this argument cannot be extended to all drop impact situations in general.

4.2. *Maximum Spread Factor.* Clanet [2] argues that, for fluids with low viscosities, ξ should scale with $We^{1/4}$. However, despite the fact that both ethanol and water have low dynamic viscosities, Figure 9 shows that such a scaling relation does not provide a good fit when considering the water and ethanol data together, for either the first or the second impact. The ethanol data does not coincide well with the trend predicted from the water data. This might imply that there is another factor in predicting the spread factor. When looking at just the water data, as in Figure 13, a scaling relation with $We^{1/4}$ may be valid. The difference between the first and second drop's spread factors appears to be constant. An estimate for this difference can be found using a basic conservation of mass argument (i.e. conservation of volume, given a constant density).

If the lamella is approximated by a cylinder of diameter d_{max} and height h, then conservation of volume would imply

$$2\pi h d_{max}^2 = \pi \frac{4d^3}{3},$$

giving a maximum spread factor for the first drop of

$$\xi_1 = d_{max}/d = \sqrt{\frac{2}{3\tilde{h}}},$$

where $\tilde{h} = h/d$ is the non-dimensional lamella thickness. The change in height of the lamella between the first and second impact can be assumed to be negligible, given that the shape of the lamella is a puddle and so h is approximately the capillary length. Then conservation of volume gives

$$2\pi h d_{max}^2 = 2\pi \frac{4d^3}{3},$$

and a maximum spread factor for the second drop of

$$\xi_2 = \sqrt{\frac{4}{3\tilde{h}}}.$$

The change in spread factors between the first and second drop impacts is then given by the difference

$$\Delta\xi = \xi_2 - \xi_1 = \left(\sqrt{\frac{4}{3}} - \sqrt{\frac{2}{3}}\right)\sqrt{\frac{1}{\tilde{h}}}.$$

For the experiments that used water, $h \approx 0.5$ mm and $d \approx 3.78$ mm, giving $\Delta\xi \approx 0.93$.

Figure 13 shows a test of this prediction for the water data. A curve was fit to the maximum spread factor data of the second impact, following the $\mathrm{We}^{1/4}$ prediction. Using the same slope, a curve was fit to the data for of first drop. This ensures a constant difference between the curves, which was given as $\Delta\xi \approx 0.900$. This agrees well with our predicted $\Delta\xi$.

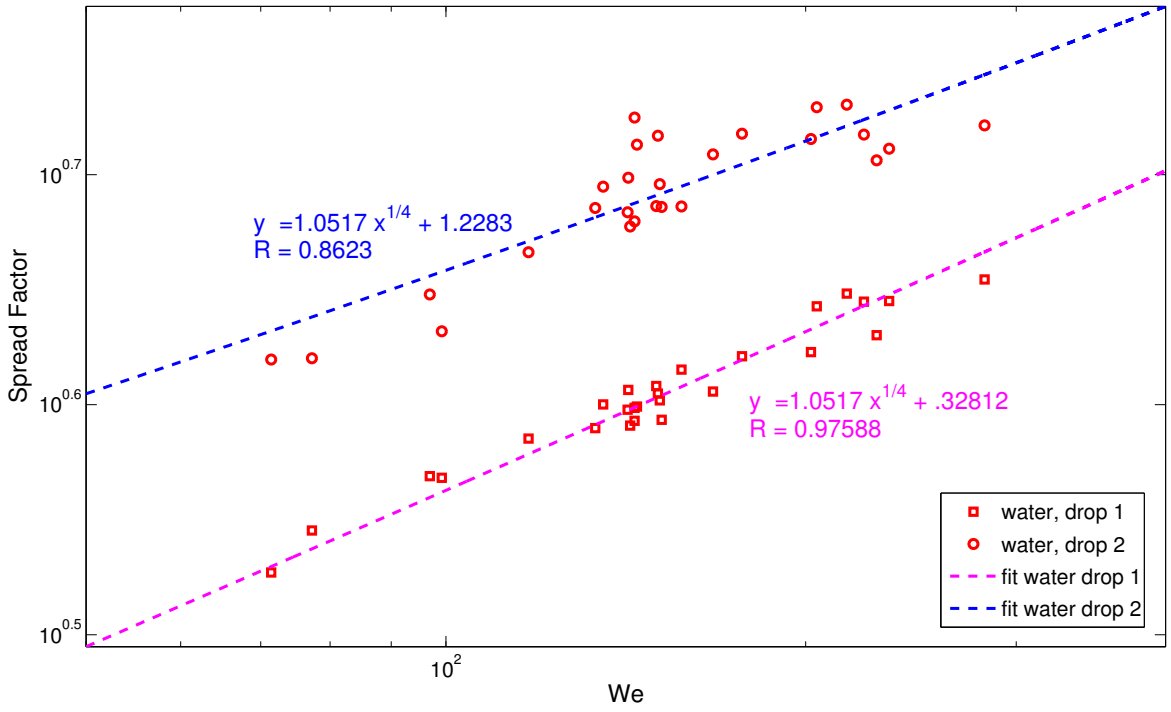

FIGURE 13. Determining the difference in spread factors between the first and second drops for water. The second drop data was fit with a scaling of $We^{1/4}$. Using this slope, a curve was fit to the first drop data.

4.3. *Splashing Behavior.* Marmanis and Thoroddsen [3] predict the number of fingers to scale with $We^{3/16}Re^{3/8}$. It seems reasonable to assume this scaling relationship might also hold for the number of secondary droplets seen during splashing since these result from disconnected fingers. As Figure 10 shows, this relationship does not accurately predict the number of secondary droplets when using multiple liquids. We instead propose that the number may scale with $(WeRe)^{3/16}$, as plotted in Figure 11. As shown in the figure, experimental variations between days (i.e. temperature and humidity) and between trials (i.e. drop size, initial velocity, etc.) cause a large discrepancy when trying to predict a trend for the number of secondary droplets. When considering such variations, the splashing thresholds and higher values seem to agree fairly well between the ethanol data and the water data from different days when using this scaling. Although the splashing threshold cannot be exactly resolved, it appears to lie in $(WeRe)^{3/16} \in [13, 13.5]$.

5. CONCLUSION

Our data supports a positive, linear correlation between the impact velocity of a drop and the spread velocity of the lamella after impact, in the range of Weber Numbers between 100 and 600. This suggests that the impact velocity of a liquid drop can describe behavior such as spreading, splashing, the formation of fingers, and other such phenomena intuitively related to spread velocity. We have also described the difference in maximum spread factors between the first and second drop impacts. Finally, we have shown that the number of secondary droplets does not appear to scale as $We^{3/16}Re^{3/8}$ as one might expect since this is the proposed scaling of the number of fingers by Marmanis and Thoroddsen. Based on our experimental data, we have instead proposed the number of secondary droplets for successive drop impacts to scale with $(WeRe)^{3/16}$.

6. Future Directions

We would like to use a larger variety of fluids to gain insight into how the measured quantities vary with fluid properties. We would also like to find a relationship which predicts the spread velocity based on the impact velocity and other fluid properties. We would like to explore what could affect the scaling of the maximum spread factor other than We. Finally, a theoretical analysis of splashing phenomena might help offer some insight into how the number of secondary droplets scales with respect to the Reynolds and Weber numbers for two successive drop impacts.

References

[1] Brown, D. (2011). Tracker: Video analysis and modeling tool. GNU General Public License. URL `http://www.cabrillo.edu/ dbrown/tracker/`

[2] Clanet, C., Beguin, C., Richard, D., & Quere, D. (2004). Maximal deformation of an impacting drop. *Journal of Fluid Mechanics*, *517*, 199–208.

[3] Marmanis, H., & Thoroddsen, S. (1996). Scaling of the fingering pattern of an impacting drop. *Physics of Fluids*, *8*(6), 1344–1346.

[4] Roisman, I., Rioboo, R., & Tropea, C. (2002). Normal impact of a liquid drop on a dry surface: model for spreading and receding. *Proceedings of the Royal Society of London*, *458*, 1411–1430.

[5] Worthington, A. M. (1908). *A Study of Splashes*. Longmans, Green, and Co.

[6] Yarin, A. (2006). Drop impact dynamics: Splashing, spreading, receding, bouncing... *Annual Review of Fluid Mechanics*, *38*, 159–192.

Source Code 1 process_ area.m

```
function process_radii(fname)
  I  = imread(fname);
  I = edge(I,'roberts');
  se = strel('disk',8);
  I = imdilate(I,se);

  % find biggest connected component
  cc = bwconncomp(I);
  n = size(cc.PixelIdxList);
  n = n(2);
  max = 0; max_el = 0;
  for ii=1:n
    s = size(cc.PixelIdxList{ii});
    if( s(1) > max )
      max_el = ii;
      max = s(1);
    end
  end

  % remove other connected components
  for ii=1:n
    if(ii ~= max_el)
      I(cc.PixelIdxList{ii}) = 0;
    end
  end

  % undilate it
  I = imfill(I,'holes');
  I = imerode(I,se);
  imshow(I);

  % display area in pixels
  sum(sum(I2))
end
```